Available online at www.sciencedirect.com
ScienceDirect
Proceedings of the Combustion Institute 31 (2007) 685–691
Proceedings of the Combustion Institute
www.elsevier.com/locate/proci

Soot particulate size characterization in a heavy-duty diesel engine for different engine loads by laser-induced incandescence

B. Bougie [1], L.C. Ganippa [2], A.P. van Vliet, W.L. Meerts, N.J. Dam *, J.J. ter Meulen

Applied Molecular Physics, Institute for Molecules and Materials (IMM), Radboud University Nijmegen, Toernooiveld 1, 6525 ED Nijmegen, The Netherlands

Abstract

Time-resolved laser-induced incandescence was used to estimate primary particle size distributions inside the combustion chamber of a heavy-duty diesel engine as a function of the crank angle, for two different engine loads at two different probe locations. Assuming a log-normal particle size distribution, an increase of the mean primary particle size was seen during the first stages of the combustion cycle, followed by a decrease later on during the combustion process.

Keywords: Laser-induced incandescence; Diesel engine; Soot; Particulate size

1. Introduction

Soot is a generally undesired byproduct of combustion. Due mainly to its negative impact on people's health it recently received increased political interest, which has resulted in legislation specifically aimed at reducing the fine-dust component in air. In the Netherlands, for instance, this has recently led to cancellation or postponing of construction works, because the cap for fine dust could not be met.

Automotive Diesel engines are a main source of fine particulates. Although much effort has already been devoted to unraveling the soot formation processes in Diesel combustion [1–3], engines provide a still badly understood environment.

Most studies on the effect of engine operating conditions on soot characteristics have focused on the exhaust gas (see e.g., Mathis et al. [4] for a recent example). Recently, Kock et al. [5] published a paper on particle size measurements with single-color Time-resolved laser-induced incandescence (TR-LII) within a light-duty, 2-stroke diesel engine. They found good agreement between the particulate size distributions in exhaust gas obtained by TR-LII and independently by a DMPS system (Differential Mobility Particle Sizer), lending credit to both the experimental method and their data evaluation model. During

* Corresponding author. Fax: +31 24 365 3311.
E-mail address: N.Dam@science.ru.nl (N.J. Dam).
[1] Present address: Delft University of Technology, Multi-Scale Physics, Delft, The Netherlands.
[2] Present address: Brunel University, School of Engineering and Design, London, UK.

1540-7489/$ - see front matter
doi:10.1016/j.proci.2006.08.040

combustion, the particle size distribution was found to vary only little in the 22–90° crank angle range.

Our paper focuses on the experimental determination of the particulate size distribution inside the combustion chamber of a heavy-duty 4-stroke Diesel engine, using a similar data evaluation procedure for the TR-LII data as Kock et al. [5]. In this model the time-dependent LII intensity is interpreted in terms of spherical primary particles; agglomeration of primary particles, an issue of current debate [12], is not considered here.

In the current study we use two-color pyrometry to estimate the temperature of the soot particles immediately after the laser pulse, and take the finite time resolution of the measurement setup, which is of the same order as the LII decay times, explicitly into account. We also compare different engine loads and different probe volume locations. Below, we briefly describe the principles of the method and our data evaluation model. Subsequently, the experimental setup is described, and the results are presented and discussed.

2. Time-resolved laser-induced incandescence

The basic idea behind laser-induced incandescence (LII) is to quickly heat particulates by irradiation with a short (~ns) laser pulse, and to record the resulting transient radiation increase. In Time-Resolved LII (TR-LII), the glowing soot is monitored by a fast detector (photomultiplier tube + sampling oscilloscope, in general). The temporal behavior of the incandescence intensity is then to be interpreted, using a model description of the energy balance. Basically, smaller particles cool faster than larger ones, so that the decay 'constant' of the LII transient contains information on the particle size distribution.

Several models for the interpretation of TR-LII data have been published, including various contributions to the particle energy loss besides radiation [5,7–11]. In fact, radiative energy loss is usually negligible in terms of energy, but of course it does provide the data for the measurements. The most sophisticated model to date is that of Michelsen [11]. A review paper about the state of the art of LII has been written by Schulz et al. [12]. A comparison of the analysis of measured LII curves at elevated pressures with several models is provided by Dreier et al. [13].

In our experiments, we deliberately keep the excitation laser intensity at a low level, in order to reduce the importance of several cooling mechanisms that operate at high particle temperatures or high incident light intensities. The model we use for data interpretation is that of Roth and coworkers [5,10], because that is, to our best knowledge, the only model that takes into account the pressure dependence in both conductive and sublimative cooling by introduction of the Knudsen number. It will be described only briefly here.

The energy balance equation for a single, spherical primary soot particle is written as [10]

$$\frac{\mathrm{d}(m_\mathrm{p} c_p T_\mathrm{p})}{\mathrm{d}t} = \dot{q}_\mathrm{abs} - \dot{q}_\mathrm{cond} - \dot{q}_\mathrm{subl} - \dot{q}_\mathrm{rad}. \tag{1}$$

The left hand side describes the time rate of change of the internal energy of a soot particle with mass m_p and specific heat c_p at an instantaneous temperature T_p. All these parameters may in principle depend on time. The terms on the right hand side of Eq. (1) describe various energy gain and loss mechanisms. $\dot{q}_\mathrm{abs}$ models the absorbed laser pulse energy, $\dot{q}_\mathrm{cond}$ the heat loss by thermal conduction, $\dot{q}_\mathrm{subl}$ the heat loss due to sublimation, and $\dot{q}_\mathrm{rad}$ the radiative heat loss. Heat transfer terms for oxidation, melting, annealing and non-thermal photodissociation like proposed by Michelsen [11] are not present in the model. Based on Michelsen's account, we expect that our model encompasses the dominant cooling mechanisms under the conditions present in a Diesel engine. As stated above, agglomeration effects are not considered in the model, and the data are interpreted in terms of spherical primary particles.

Under the conditions prevalent in the Diesel engine, the heat loss is dominated by the conduction term [14]. The conduction term is more important under high-pressure conditions because it is inversely proportional to the Knudsen number [15], which is small in typical engine environments. The sublimation term, however, is less important under high-pressure conditions, because it is proportional to the Knudsen number [15]. For the particle heat loss the radiation term is negligible as well, but of course the instantaneous temperature is decisive for the radiative power, which is the quantity that is detected experimentally. During the combustion stroke, pressure and temperature within the combustion chamber vary to such an extent that the conduction heat loss term must be modeled in various flow regimes. This is incorporated in the model by including a Knudsen-number dependent interpolation function in the conduction heat loss term. This interpolation function provides a smooth transition between the heat loss terms in the continuum regime and the free molecular regime [10,14,15]. The temperature of the bath gas in which the laser-heated particles cool down is assumed to be equal to the mean gas temperature, as evaluated from the ideal gas law and the time-dependent pressure in the combustion chamber (see Section 3). The wavelength-dependent radiative power emitted by a particle at temperature T_p follows from Planck's law as

$$P_\mathrm{rad}(\lambda) = \lambda^{-5}\left(\exp\left\{\frac{hc}{\lambda k T_\mathrm{p}}\right\} - 1\right)^{-1} \varepsilon_\lambda(\lambda) \tag{2}$$

in which the absorption coefficient ε_λ accounts for gray-body effects. In our experiments, the LII signal is detected through narrow-band colored glass filters, and we evaluate Eq. (2) at a single wavelength in the center of each filter's transmission curve. An important aspect in the data interpretation is that under the pressure and temperature conditions within the engine, the decay time of the incandescence intensity is so short (ca. 20 ns) that the finite response time of the detection system (~10 ns) and the finite duration of the excitation laser pulse (~8 ns) can no longer be neglected. Essentially, the detected LII power is a convolution of three time-dependent terms, viz. the laser pulse intensity, the LII power as if it were excited by an infinitely short laser pulse, and the detection system time response. We extract clean temporal LII decay curves from the raw data by deconvolution with a system response function (see Section 4).

3. Experimental setup

Experiments were performed on a six-cylinder, heavy-duty Diesel engine, with a compression ratio of 15. The intake air of the measurement cylinder was at a temperature of 313 K. One of the cylinders was modified to provide optical access for *in situ* measurements. The configuration of the measurement cylinder and the optical arrangement used for the TR-LII measurements are shown in Fig. 1.

Optical access was obtained by replacing the original piston and cylinder by a liner arrangement including several windows and an extended piston with a quartz bottom. This piston window provides a wide field of view from below into the combustion chamber. Besides this, a quartz window in the top of the cylinder wall provides a side view of the combustion chamber. One of the exhaust valves has been replaced by a quartz window to enable laser beams to pass top-down through the engine. The piston crown was provided with a slot to enhance optical access through the side window in the early phase of the combustion cycle. To reduce fouling of the quartz windows by soot, no lubricants were used to operate the engine. The engine is equipped with an in-line pump (start-of-injection at 5° bTDC), and runs on commercial, low-sulphur city-Diesel fuel. Soot measurements were performed at two positions: between two sprays and through a spray (closed circle and open circle, respectively, as indicated in Fig. 2).

The fundamental wavelength of a pulsed Nd:YAG laser ($\lambda = 1064$ nm) was used to heat the soot inside the combustion chamber through the valve window. A laser fluence of 0.25 J/cm^2 (at the entrance window) was chosen to minimize fluctuations of the LII signal. Incandescence of the laser-heated soot particles was observed through the side window, both by an imaging grating spectrograph and by two band-pass-filtered photomultiplier tubes (PMTs). The entrance slit of the spectrograph was kept fully open to increase signal strength. An intensified CCD camera mounted on the exit port was used to read out spectra of the LII signal. In separate experiments, the prompt LII signal was recorded over the wavelength range from 310 nm to 610 nm for successive injections. During each individual injection the spectrograph covered a range of 30 nm. In this way it was revealed that there was no interference from any other species (precursors of soot, or Swan band emission of C_2) for the chosen excitation wavelength.

The TR-LII radiation was filtered by a Schott BG-18 filter, and imaged onto the PMTs by two spherical lenses. By using a beamsplitter the LII was split into two different beams and detected by two PMTs (Thorn EMI). The light registered by the PMT of type 9814QB was additionally filtered by a Schott BG-1 filter before detection, and the light detected by the PMT of type

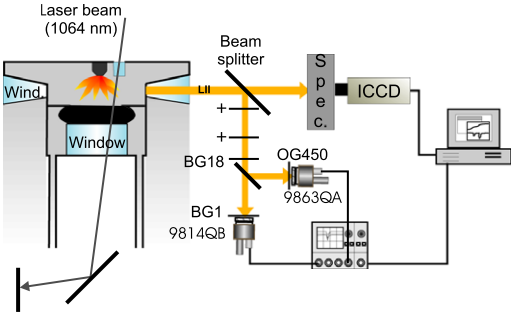

Fig. 1. Schematic picture of the modified cylinder. Windows have been inserted in the cylinder, through which the laser light is guided down. The LII signal is detected through the side-window.

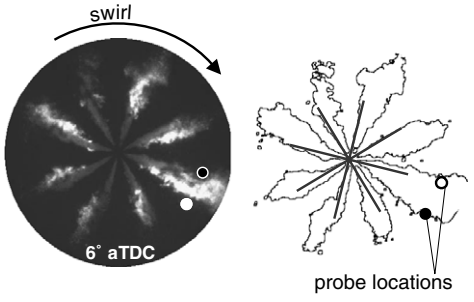

Fig. 2. Natural luminosity image recorded through the piston window, with indication of the two probe locations in the engine. At the right a contour plot in which the spray axes are indicated.

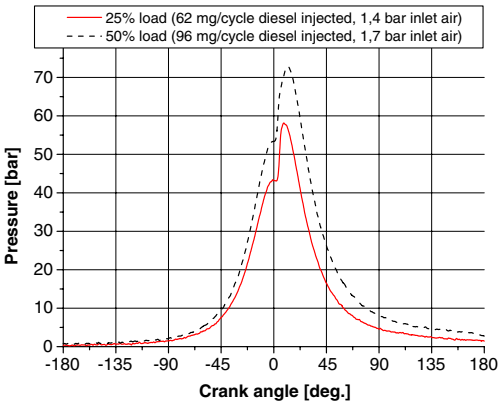

Fig. 3. Pressure curves for the selected engine loads.

9863QA was filtered by a Schott OG-450 filter. This resulted in two central detection wavelengths of 370 nm (FWHM 40 nm) and 560 nm (FWHM 50 nm), respectively, taking into account the spectral sensitivity of the PMTs. The detected TR-LII signal from the PMTs was displayed on a 300 MHz digital oscilloscope (Lecroy 9630; 2.5 Gs/s), digitized, and stored and analyzed on a PC.

TR-LII measurements were performed for two engine loads; the corresponding cylinder pressures are shown in Fig. 3. The low engine load, from now on called 25% load, consisted of a boost pressure of 1.4 bar, inlet air temperature of 313 K, and 62 mg fuel injected per cycle (injection duration 10°). The higher engine load, from now on called 50% load, consisted of a boost pressure of 1.7 bar, inlet air temperature of 313 K, and 96 mg fuel per injection (duration 14°). In both cases, the engine ran at 1430 rpm, and the measurement cylinder was skip-fired (1:35, or about once per 3 s).

4. Results and discussion

Laser-induced incandescence was simultaneously measured by two different PMTs, covering disjunct wavelength ranges. In the Rayleigh limit the temperature immediately after the laser pulse is independent of the particle size [16], but it does, of course, depend on the local laser power. It was calculated from the ratio of the peak intensities of both PMT readings (2-color pyrometry) to provide an initial temperature for the fit of the measured TR-LII curves [17]. The initial temperature varied between 2200 K and 3800 K, probably as a result of variations in available laser intensity in the probe volume, due to beam profile and in-cylinder attenuation. However, the initial temperature has been shown not to be very critical for the calculation of the particle sizes from the TR-LII curves [18], at least under the conditions that exist within the Diesel engine.

Under the conditions prevalent in the engine, the LII intensity decay was found to be so fast that the response time of the detection system and the finite duration of the laser pulse could not be neglected. Therefore, a Wiener deconvolution was implemented, which corrected the measured curves for the response time of the detection system (see Fig. 4).

Without deconvolution of the signal the estimated soot particle size would be about 10% bigger. The measured, deconvolved curves were fitted using the model of Kock and Roth [10] for the transition regime, assuming a log-normal particle size distribution for the soot particles. The latter is defined as

$$P(r) = \frac{1}{\sqrt{2\pi}\sigma_m r} \exp\left\{-\frac{(\ln r - \ln r_m)^2}{2\sigma_m^2}\right\}, \qquad (3)$$

in which r is the radius of a particle, r_m is the mean particle radius and σ_m is the width of the size distribution.

For each crank angle and each engine setting the measurement cylinder was fired 20 times. LII signal was observed for only part of the injections. Typically 2–6 injections out of 20 resulted in LII signal on both PMTs and on the spectrograph (Fig. 5). For the other injections no signal was observed, or, in rare cases, an LII-like signal was observed on only one of the PMTs and not on the spectrograph. These were regarded as spurious, and not included in the analysis. The relative paucity of useful LII data indicates that the soot formation in our engine is far from uniform and non-reproducible on the scale of our probe volume (estimated height = 10 mm, diameter = 5 mm).

In Fig. 6 the results of the radius as a function of the CA are presented for the different probe locations. Each data point corresponds to one instantaneous measurement (single laser pulse). In addition, the average value for the radius has

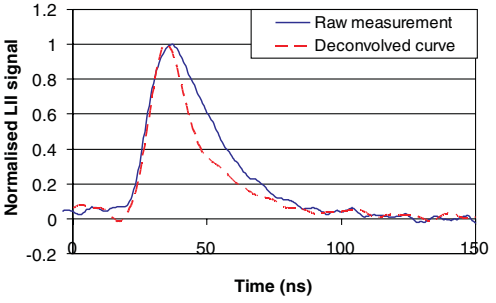

Fig. 4. Example of the influence of the deconvolution on the measurement data.

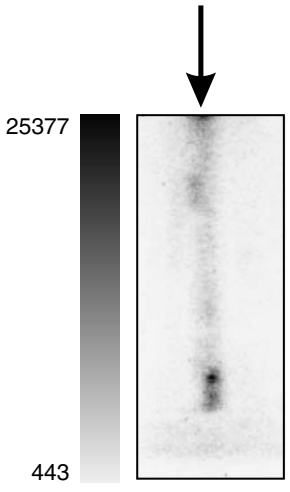

Fig. 5. Image of line with glowing soot, which was hit by the laser, recorded through the side window. The gray scale indicates the intensity of the image, in arbitrary units. The arrow indicates the path of the laser beam.

been plotted together with the standard error of r_m defined as

$$\mathrm{SE} = \frac{\sigma_{\mathrm{std}}}{\sqrt{N}}, \tag{4}$$

in which σ_{std} is the standard deviation of the N measurements. The values for σ_m were all found to fall in the range from 0.25 to 0.35 (corresponding to a FWHM of the particle radius distribution of 10–35 nm, depending on the value of r_m). The fitted radii for the individual measurements have been plotted in the four different graphs. An analysis of variance (ANOVA) showed that within a confidence interval of 95% the particle size cannot be considered to be constant as a function of crank angle for all engine conditions considered here.

The general trend in the mean particle size is shown by the trend lines in Fig. 6. It can be seen that the particle sizes increase during early stages of the combustion cycle and later on decrease again. Considering the 25% load case, it can be said that the particle size varies much more with crank angle for the 'through spray' than for the 'between sprays' location. Based on the trend lines in Fig. 6 it follows that in the 'through spray' location the maximum mean particle radius is a bit larger (45 nm) and reached a bit earlier in the stroke (at ca. 50° aTDC) than in the 'between sprays' location (40 nm and ca. 70° aTDC, respectively). The particle radii have not yet converged to the same limit at 100° aTDC, indicating that the cylinder contents are not yet completely mixed by that time. For the 50% load case, maximum mean particle sizes and the crank angles at which they occur are similar, but the scatter in data

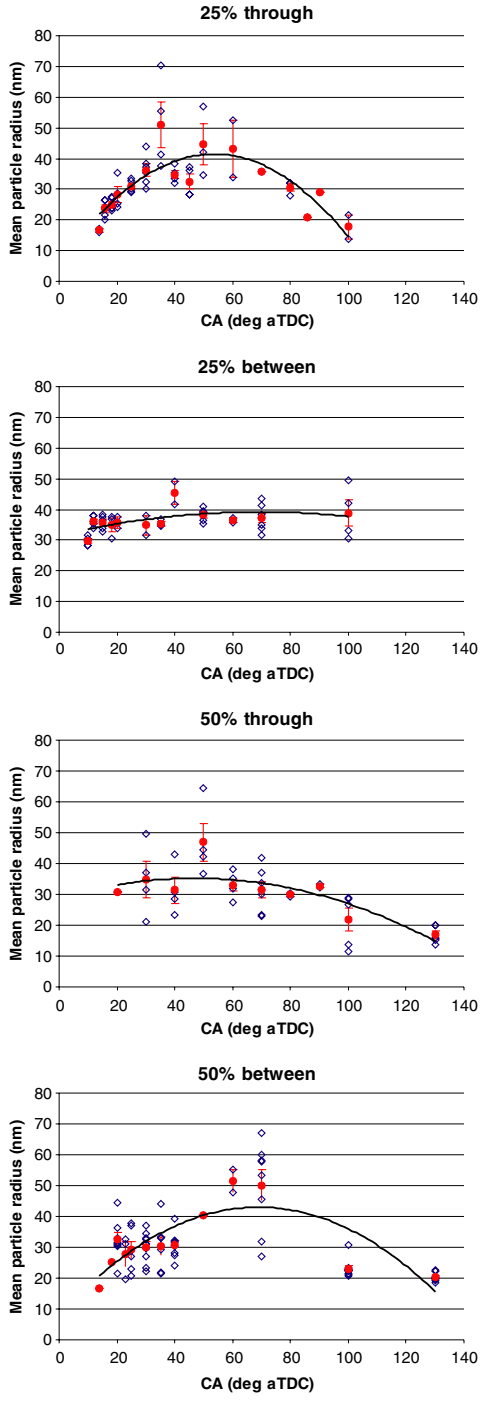

Fig. 6. Mean particle size as a function of crank angle for the different engine loads and different probe locations. The open rhombi indicate the separate measurements, and the closed circles indicate the average values of the measurements during each cycle. The error bars around the latter indicate the standard error in the measurements. Trend lines have been included in all graphs.

points is larger than in the 25% load case. The latter is probably due to increased attenuation. (Although signal strength should not affect the decay times, there is of course a S/N issue.)

Particle sizes could not be derived before 10° aTDC in the 25% load case, and before 18° aTDC in the 50% load case. This early in the stroke, the LII intensities were below our detection limit. Late in the stroke (above ca. 100° aTDC) the LII intensities also declined, resulting in useful data only for the 50% load case. From Fig. 3 it follows that combustion starts at about 1° aTDC, and maximum heat release occurs at 5° aTDC in the 25% load case and at 3° aTDC in the 50% load case. The lower limits for the crank angle at which soot could be detected correspond closely to the maxima in the pressure curves.

The trend lines included in Fig. 6 show some variation for the four measurement series. In the 25% load 'through spray' and the 50% 'between sprays' cases the mean particle size r_m starts small, goes through a maximum and declines again with increasing crank angle. For the other two cases, this behavior is suggested, but much less evident. Several explanations are available for such a trend. Speaking strictly in engine terms (see e.g., Heywood [19]), soot particles are expected to be formed from scratch, so to start small, then to grow in size and number as the combustion stroke proceeds, but to decrease in size (and number?) again later in the stroke, as the formation has stopped but the oxidation continues. This course of events is roughly in agreement with the trends observed in Fig. 6, although the maxima occur a bit late in the stroke (see e.g., [20]). There are, however, also some experimental issues, although these are more speculative. On the one hand, the contribution of individual laser-heated particles to the LII signal scales with the square of the radius (surface emitters). Thus, LII is predominantly sensitive to the larger particles. This is to some extent taken into account by the assumption of a particle size distribution, but it should be kept in mind that the actual shape of the distribution is not known. On the other hand, Diesel soot exists as agglomerates of more-or-less spherical primary particles. Although LII is often claimed to yield information on only the primary particle size, the compactness of the particles is not irrelevant [6]. Loose, chain-like aggregates will be represented more accurately by the sum of the individual primary particles than do compact, ball-like agglomerates (see the TEM pictures in Vanderwal [21] and Kock [5]). Thus, the curves in Fig. 6 are biased towards larger primary particles, and may also reflect the effect of agglomeration during the early combustion phase, rather than actual growth of primary particles. Similarly, the decline of the curves later in the stroke can indicate the oxidation of primary particles or agglomerates, but also the break-up of agglomerates into smaller and perhaps less compact fragments. There is some indication that at least later in the stroke (the exhaust valve opens at 130° aTDC) the LII data do indeed represent primary particle sizes, as they compare well with TEM data on Diesel soot [5,22].

The only other study of in-cylinder Diesel soot particles known to us [5] has shown similar trends and size distributions, with relatively little variation as a function of crank angle. Unfortunately, type of fuel and probe volume location relative to the sprays are not indicated in this paper.

5. Conclusions

Two-color Time-resolved Laser-induced incandescence (TR-LII) measurements have been performed in a production-type heavy-duty Diesel engine running on low-sulphur 'city diesel' fuel. The prompt LII signal measured in two disjunct wavelength bands was used to estimate the initial temperature of the Nd:YAG-laser-heated soot particles. The finite duration of the laser pulse and the detection system have been taken into account explicitly by deconvolution. When interpreted in terms of primary particle sizes, the trends observed under conditions of different engine load and probe volume location indicate that the mean particle radius first grows to about 40 nm, and then decreases with increasing crank angle.

Issues to be addressed in future experiments are the bath gas temperature (now taken to be the global mean gas temperature), the definition of the probe volume (by spatial filtering, for instance) and the model description of the energy balance.

Acknowledgments

The authors are very grateful for the help in the modeling part from B. Kock and P. Roth. This research is supported by the Technology Foundation STW, applied science division of NWO and the technology programme of the Dutch Ministry of Economic Affairs.

References

[1] D.B. Kittelson, *Journal of Aerosol Science* 29 (5/6) (1998) 575–588.
[2] D. Siebers, D. Higgins, *SAE Paper* 2001-01-0530, 2001.
[3] G. Bruneaux, *COMODIA 2001* (2001) 622–630.
[4] U. Mathis, M. Mohr, R. Kaegi, A. Bertola, K. Boulouchos, *Environmental Science and Technology* 39 (6) (2005) 1887–1892.
[5] B.F. Kock, Th. Eckhardt, P. Roth, *Proc. Combust Inst* 29 (2) (2002) 2775–2781.
[6] F. Liu, G.J. Smallwood, D.R. Snelling, *Journal of Quantitative Spectroscopy & Radiation Transfer* 93 (1–3) (2005) 301–312.

[7] S. Will, S. Schraml, K. Bader, A. Leipertz, *Applied Optics* 37 (24) (1998) 5647–5658.
[8] G.J. Smallwood, D.R. Snelling, F. Liu, Ö.L. Gülder, *Journal of Heat Transfer* 123 (4) (2001) 814–818.
[9] H. Bockhorn, H. Geitlinger, B. Jungfleisch, et al., *Physical Chemistry Chemical Physics* 4 (15) (2002) 3780–3793.
[10] B.F. Kock, P. Roth, *Proceedings of the European Combustion Meeting 2003* (2003) 093.
[11] H. Michelsen, *Journal of Chemical Physics* 118 (15) (2003) 7012–7045.
[12] C. Schulz, B.F. Kock, M. Hofmann, et al., *Applied Physics B: Lasers and Optics* 83 (2006) 333–354.
[13] T. Dreier, B. Bougie, N. Dam, T. Gerber, *Applied Physics B: Lasers and Optics* 83 (2006) 403–411.
[14] B. Bougie, L.C. Ganippa, A.P. van Vliet, et al., *Proceedings of the European Combustion Meeting 2005* (2005) 166.
[15] M.M.R. Williams, S.K. Loyalka, *Aerosol Science Theory and Practice, With Special Applications to the Nuclear Industry*, Pergamon Press, Oxford, 1991.
[16] P. Roth, A.V. Filippov, *Journal of Aerosol Science* 27 (1) (1996) 99–104.
[17] S. deIuliis, M. Barbini, S. Benecchi, F. Cignoli, G. Zizak, *Combust. Flame* 115 (1–2) (1998) 253–261.
[18] B. Bougie, L.C. Ganippa, A.P. van Vliet, W.L. Meerts, N.J. Dam, J.J. ter Meulen, *Combust. Flame* 145 (2006) 635–637.
[19] J.B. Heywood, *Internal Combustion Engine Fundamentals*, McGraw Hill, 1988.
[20] G. Lepperhof, *Topics in Catalysis* 16/17 (2001) 249–254.
[21] R.L. Vanderwal, T.M. Ticich, A.B. Stephens, *Combust. Flame* 116 (1–2) (1999) 291–296.
[22] K. Park, D.B. Kittelson, P.H. McMurry, *Aerosol Science and Technology* 38 (9) (2004) 881–889.